Section A-Research paper
ISSN 2063-5346

A new organomercury compounds based on nitroanthracene: Synthesis and Characterization

Wathiq Abdul Abbas Odah[1] Nuha Hussain Al-Saadawy[1*]

[1]Department of Chemistry, College of Science, University of Thi-Qar, Thi-Qar, 64001, Iraq*

Corresponding author: e-mail: nuh.hussain@sci.utq.edu.iq
nuhaalshather@yahoo.com

Abstract

The aim of this study is to obtain organomercury compounds containing nitro group such as (10-nitroanthracen-2-yl)mercury(II) chloride and (9-nitroanthracen-2-yl)mercury(II) chloride by a mercuration reaction. The paper includes the preparation of a new organomercury compound based on nitroanthracene was prepared by mercuration reaction to 9-nitroanthracene by mercuric acetate then lithium chloride. *m*-$C_{14}H_8ClHgNO_2$ (A) and *o*-$C_{14}H_8ClHgNO_2$ (B). The prepared compounds were characterized by using FT- IR, ^{1}H NMR, ^{13}C NMR, XRD and MASS technique. The results of the chemical analysis to prepared compounds showed that it a good agreed with the proposed chemical structures. The purpose of this study to compare between meta and ortho organomercury derivatives for 9-nitroanthracene according to physical and chemical properties.

Keywords: *Organomercury, 9-nitroanthracene, ^{1}H NMR, mass spectra, mercuric chloride, mercuric acetate*

Introduction

Mercury is a chemical element, its chemical symbol (Hg) is located in the third transition period of the periodic table, the atomic number is (1), it has seven stable isotopes, and it has three oxidation states (1^+,2^+,4^+) [**2**]. Organic mercury compounds have a general formula (R-Hg-X), where R is either an alkyl radical, a phenyl group, or an alkoxyl. The first person to detect organic mercury compounds was the English scientist Edward Frankland. In 1852 AD, who prepared the first organic compound for metal mercury, dimethyl mercury (Me2Hg) by treating methyl iodide CH_3I directly with mercury [**3**]. Studies conducted on this compound proved that it is soluble in fats, which indicates its toxicity due to its bio-accumulation and rapid spread in the human body, since organic

mercury derivatives are less volatile than elemental mercury itself [**4, 5**] and mercury compounds have many industrial and medical uses such as manufacturing Mercury batteries containing mercury oxide and other industries [**6, 7**], as well as antiseptics known as (mercurochrome) [**8**]. Mercuric diacetate is the basis for the preparation of organic mercury compounds, through which mercury is introduced to organic compounds [9-17]. In this work, A new organometallic compound type organomercury derived from 9-nitroanthracene were prepared and namely (10-nitroanthracen-2-yl)mercury(II) chloride **A** and (9-nitroanthracen-2-yl)mercury(II) chloride B**,** then the x-ray diffraction of organomercury compound (A & B) has been investigated.

Experimental Section

Materials

The chemicals used in this study included ethanol absolute (BDH), lithium chloride (Sigma-Aldrich), mercuric acetate (Fluka).

Instrumentation

Infra-red spectra were recorded with KBr disks utilizing an FTIR spectrophotometer Shimadzu model 8400 S in reach 4000 - 400 cm^{-1}. The mass spectra were performed using a HAT-8200 analyzer at the ionizing potential of 70 eV (Central Laboratory, University of Tehran, Iran). The melting point was measured using the Melting point SMP 31 model. Nuclear Magnetic Resonance Spectroscopy 1H NMR within range (0-15) at the Basra University/ College of Education for pure sciences, and XRD were recorded at Central Laboratory, University of Tehran, Iran.

Procedure

Synthesis of (4-amino-[1,1'-biphenyl]-3-yl)mercury(II) chloride (A)

Firstly 50g (0.22mol) of 9- nitroanthracene was dissolved in 50 ml of absolute ethanol, then added to it 70g (0.22mol) of mercuric acetate dissolved in 50 ml of absolute ethanol, and the mixture was refluxed for 12h with the follow-up of the reaction via TLC. After the reaction was completed, 9.32g (0.22mol) of lithium chloride was added, and the reaction rose again for 1 h then the solution was filtered. Brown crystals were formed on the filter paper and then washed via hot ethanol several times to get rid of the remains of unwanted materials. The weight of produced compound was 66 g, the yield was69%, and the melting point of the compound was measured after completely drying was 187-189 ℃.

FT-IR using KBr:

ν(C–H) Aromatic=3055 cm^{-1}, ν(C–N) Aromatic=1310 cm^{-1}, ν(C=C) Aromatic=1612 cm^{-1}, ν(NH_2) = (3327 cm^{-1}, 3408 cm^{-1}).

Mass spectra: The MS calculated for A $C_{12}H_{10}NHgCl$ (404.26) was found to be as follows: M^++1(405); MS/MS (m/z): 365, 317, 277,236, 169, 154, 144, 78.

These data were shown in (Scheme1 and S1,Table3,Fig S2)

Results and discussion

In the current study, the organomercury compounds such as ArHgCl were prepared, by two steps where Ar is the 9-nitroanthracene: the first was prepared the organomercury acetate from the reaction between 9-nitroanthracene and mercuric acetate in ethanol with reflux for 12 hours, the second step was the reaction between organomercury acetate compounds with lithium chloride to produce the final compound, as shown in Scheme (1).

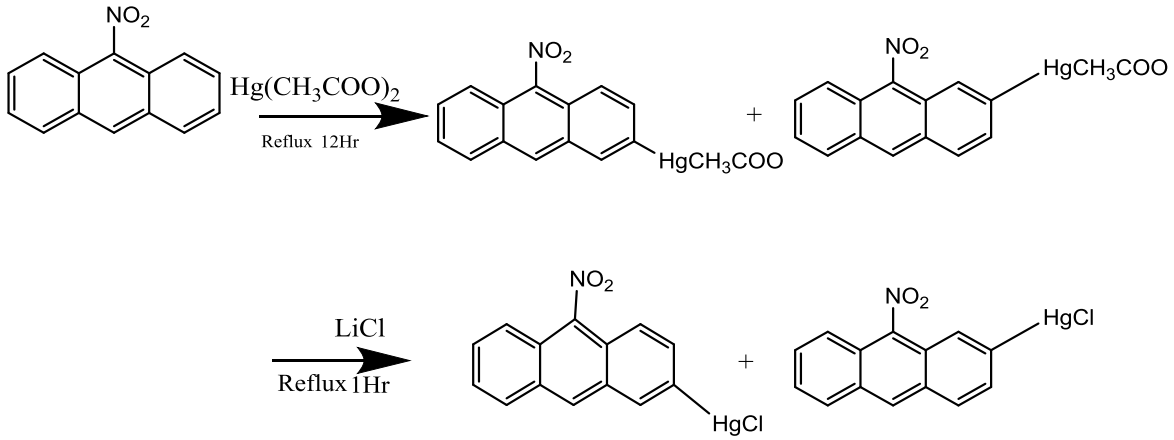

Scheme 1 Synthesis of organomercury compounds A and B

IR spectra of the compounds under study displayed standard features in specific regions and characteristic bands in the other areas explained in Table 2 .In all the compounds under study, the aromatic C-H bond appeared in the range 3007 - 3058 cm^{-1} [9-17]. The clear band in the range of 1591 and 1596 cm^{-1} respectively was attributed to the aliphatic bond C=C [9 -17]. while those spectra which showed bands at 1284 and 1317 cm^{-1} are due to the amplitude oscillation of the C–N bond [9-17]. Explained in Schemes1andS2,Table S1, and Fig S2

Table (S1) Physical data for organotellurium compounds

Co.	Molecular formula	M.Wt	Color	m.p. C°	Yield %
A	*m*-$C_{14}H_8ClHgNO_2$	459	Light brown	187 °-189 °	**69**.2%
B	*o*-$C_{14}H_8ClHgNO_2$	459	Dark brown	130 °- 132 ° D	**12**.8%

D= decompostion

Table (S2) Main absorption bands in the infrared spectra of the prepared compounds

Co.	C-H aromatic	C=C	N=O	C-N
A	3058 cm^{-1}	1591 cm^{-1}	1516 cm^{-1}	1317 cm^{-1}
B	3007-3057 cm^{-1}	1596 cm^{-1}	1516 cm^{-1}	1284 cm-1

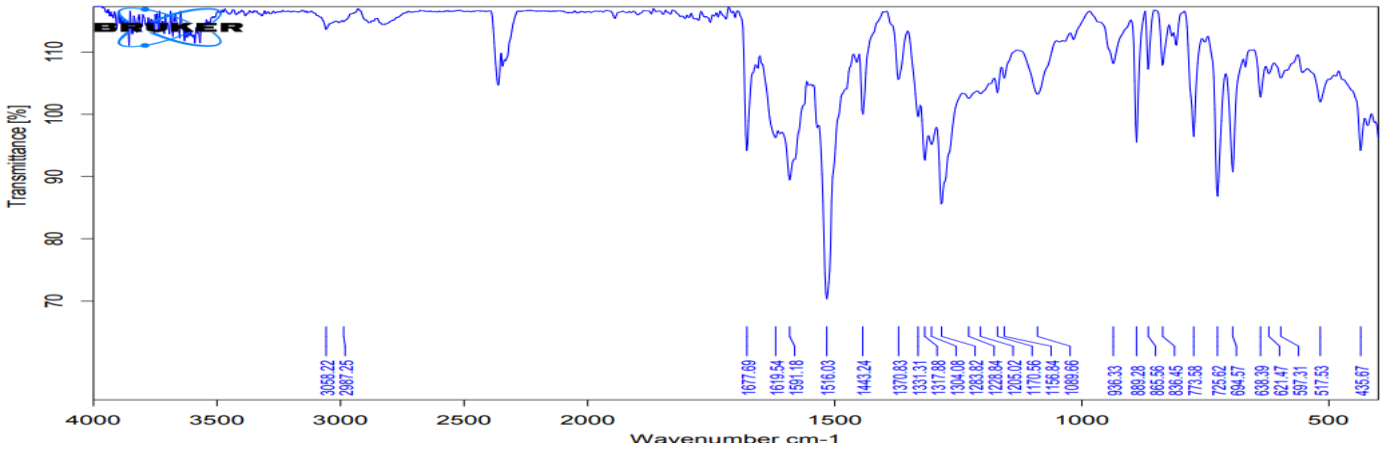

Fig S1. Infrared spectrum of the compound A

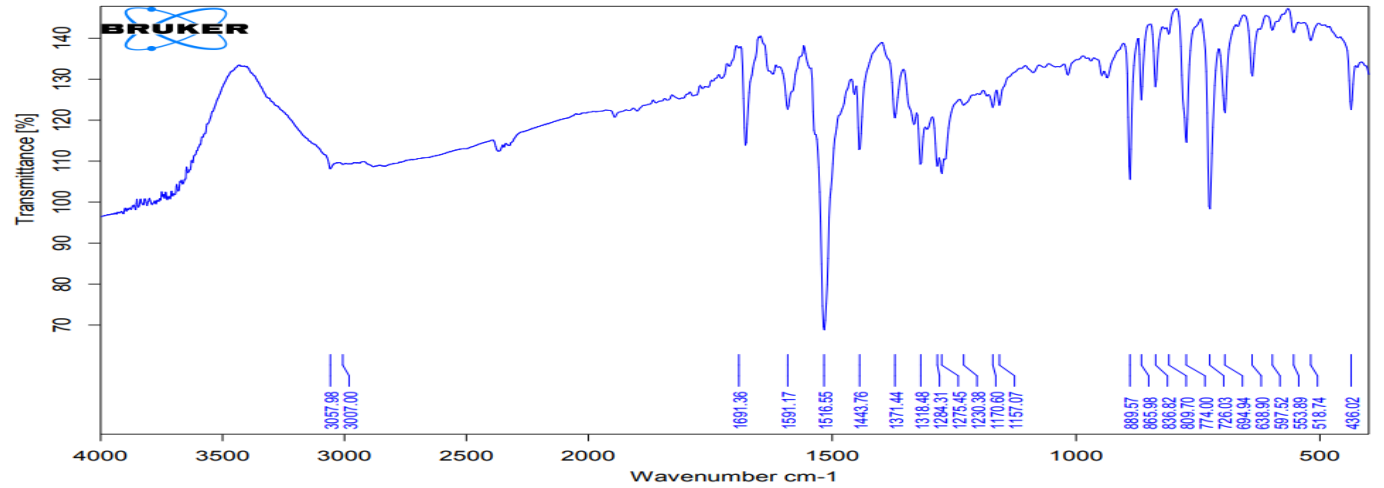

Fig S2. Infrared spectrum of the compound B

The mass spectrum of compound A

The mass spectrum showed us the appearance of the molecular ion band or the parent band at 458 m/z, which represents the molecular weight of the resulting compound, as well as the emergence of a band of high relative abundance at 202 m/z belonging to the group $(C_{12}H_{11}NO_2)^+$, which represents the main band, in addition to a group of other bands shown. In Scheme No. (S1). The mass spectrum of the compound is shown in Figure (S3).

Table(S3) The most important fissions of the compound A

Molecular ion	m/z	Molecular ion	m/z
[$C_{14}H_8NO_2HgCl$	458.26	$[C_{14}H_9HgCl]^{\cdot+}$	413.27
$[C_{14}H_9NO_2]^{\cdot+}$	223.23	$[C_{12}H_{11}NO_2]^{\cdot+}$	201.23
$[C_6H_7HgCl]^{\cdot+}$	315.16	$[C_3H_4HgCl]^{\cdot+}$	277.11
$[C_2H_3HgCl]^{\cdot+}$	263.09	$[C_{10}H_7NO_2]^{\cdot+}$	173.17
$[C_8H_7NO_2]^{\cdot+}$	149.15	$[C_4H_7NO_2]^{\cdot+}$	101.11

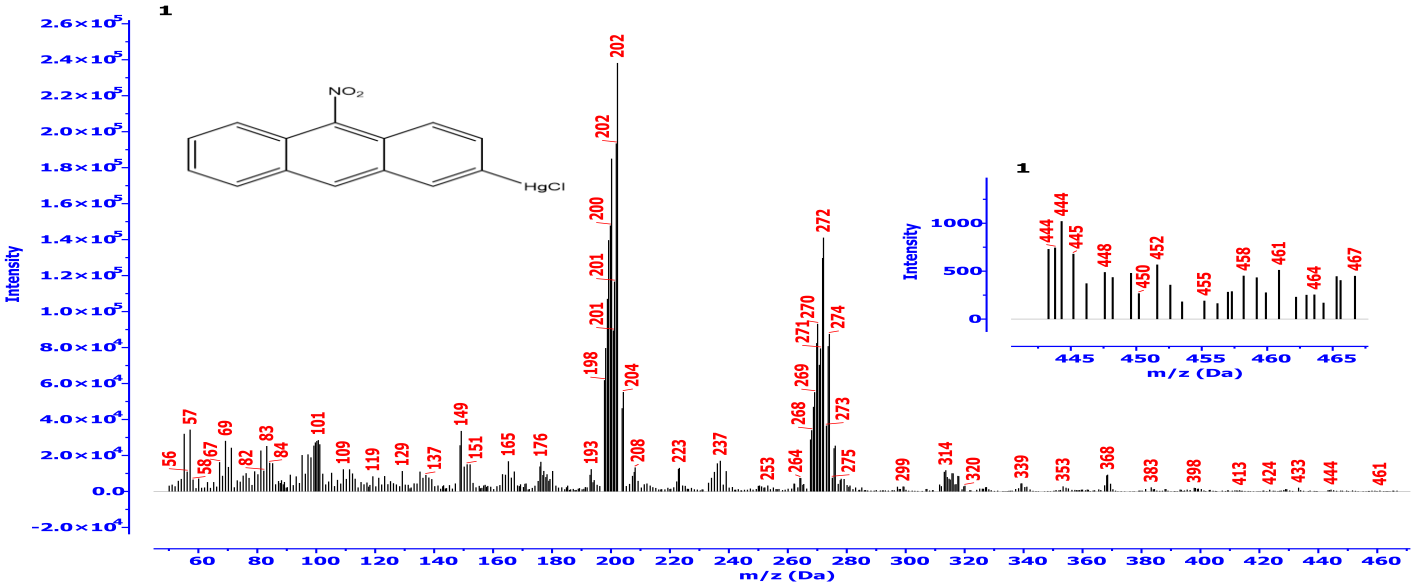

Fig S3. The mass spectrum of the compound A

The mass spectrum of compound B

The mass spectrum showed us the appearance of the molecular ion band or the parent band at 458 m/z, which represents the molecular weight of the resulting compound, as well as the emergence of a band of high relative abundance at 202 m/z belonging to the group (+C12H11NO2), which represents the main band, in addition to a group of other bands shown. In Scheme No. (S2). The mass spectrum of the compound is shown in Figure (S4).

Table(S4) The most important fissions of the compound B

Molecular ion	m/z	Molecular ion	m/z
[$C_{14}H_8NO_2HgCl$	458.26	$[C_{14}H_9HgCl]^{\cdot+}$	413.27
$[C_{14}H_9NO_2]^{\cdot+}$	223.23	$[C_{12}H_{11}NO_2]^{\cdot+}$	201.23
$[C_6H_7HgCl]^{\cdot+}$	315.16	$[C_3H_4HgCl]^{\cdot+}$	277.11
$[C_2H_3HgCl]^{\cdot+}$	263.09	$[C_{10}H_7NO_2]^{\cdot+}$	173.17

$[C_8H_7NO_2]^{\cdot+}$	149.15	$[C_4H_7NO_2]^{\cdot+}$	101.11

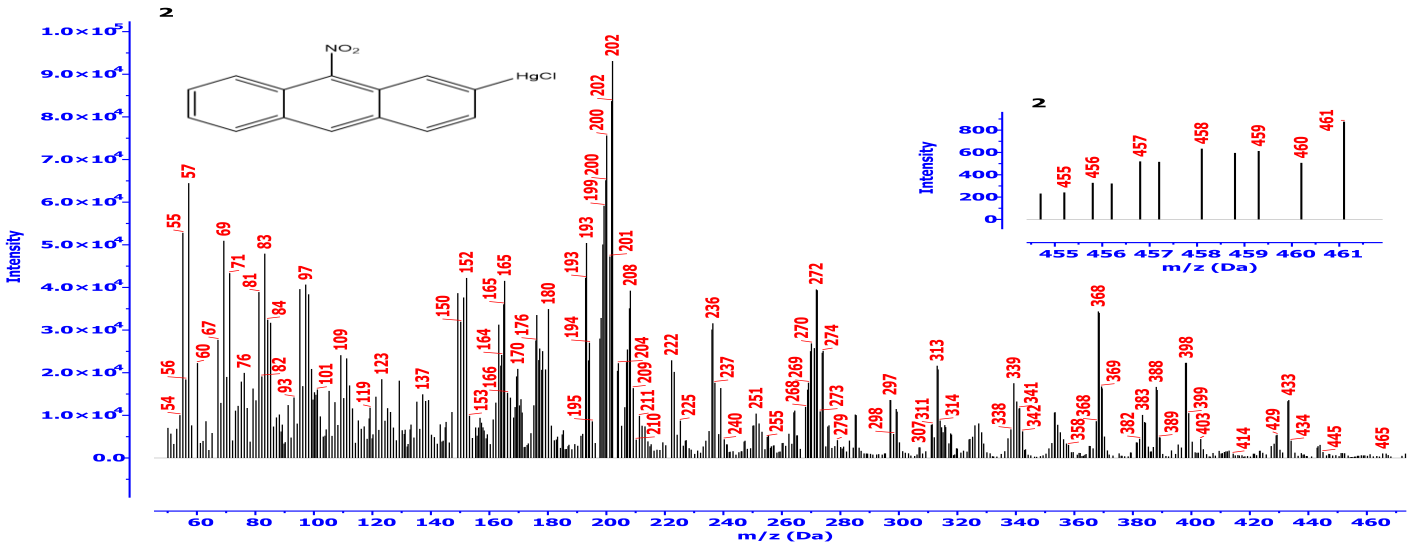

Fig S4. The mass spectrum of the compound B

Proton NMR spectra

The ^{1}H NMR magnetic resonance spectrum measurements are one of the important techniques in diagnosing the composition by inferring the location of the protons within the compound. Below is an interpretation of all the spectra of the compounds prepared in this study.

The spectrum of compound A

The H1NMR spectrum showed different bands and multiple signals in the aromatic region with offsets extending between (7.6 – 8.9) ppm, as well as the appearance of bundles with different displacements because they are not chemically equivalent to the back of a bundle mono at (8.9ppm) due to H7 (S) as well as at (8.27ppm) due to H11 (S) as wellas The appearance of a beam at (8.20ppm) returning to H6 (dd) and the appearance of a beam at (7.90) returning to H1(T), And another one at (7.68) due to H2 (T), as well as a package at (7.78ppm) returning to H14 (dd),as in the Figure (S5).

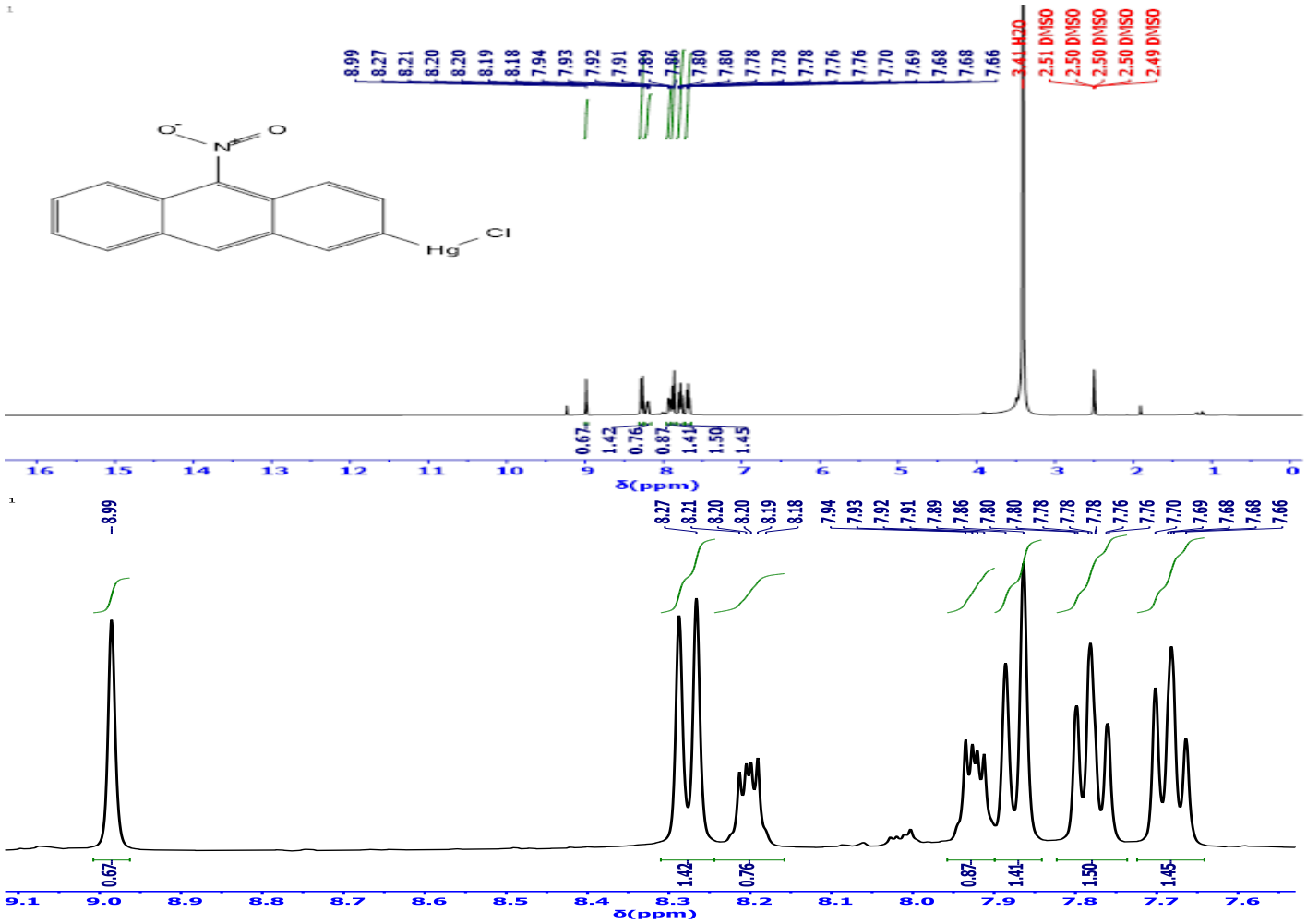

Fig S5. The ^{1}H NMR spectrum of compound A

The spectrum of compound B

The H1NMR spectrum showed different bands and multiple signals in the aromatic region, with offsets extending between (7.7-9.1 PPM .(As well as the appearance of bands with different displacements because the protons are not chemically equivalent, so a band appeared at (9.1ppm) belonging to H7 (S) As well as the appearance of a beam at (8.30ppm) returning to H6 (d), as well as the appearance of a beam at (8.22ppm) returning to H11 (dd), as well as the appearance of a beam at (7.91ppm) returning to H1 (T), and the appearance of a beam at (7.8ppm) Returning to H3 (d) as well as appearing at (7.70ppm) returning to H2 (dd) as in the figure below(S6)

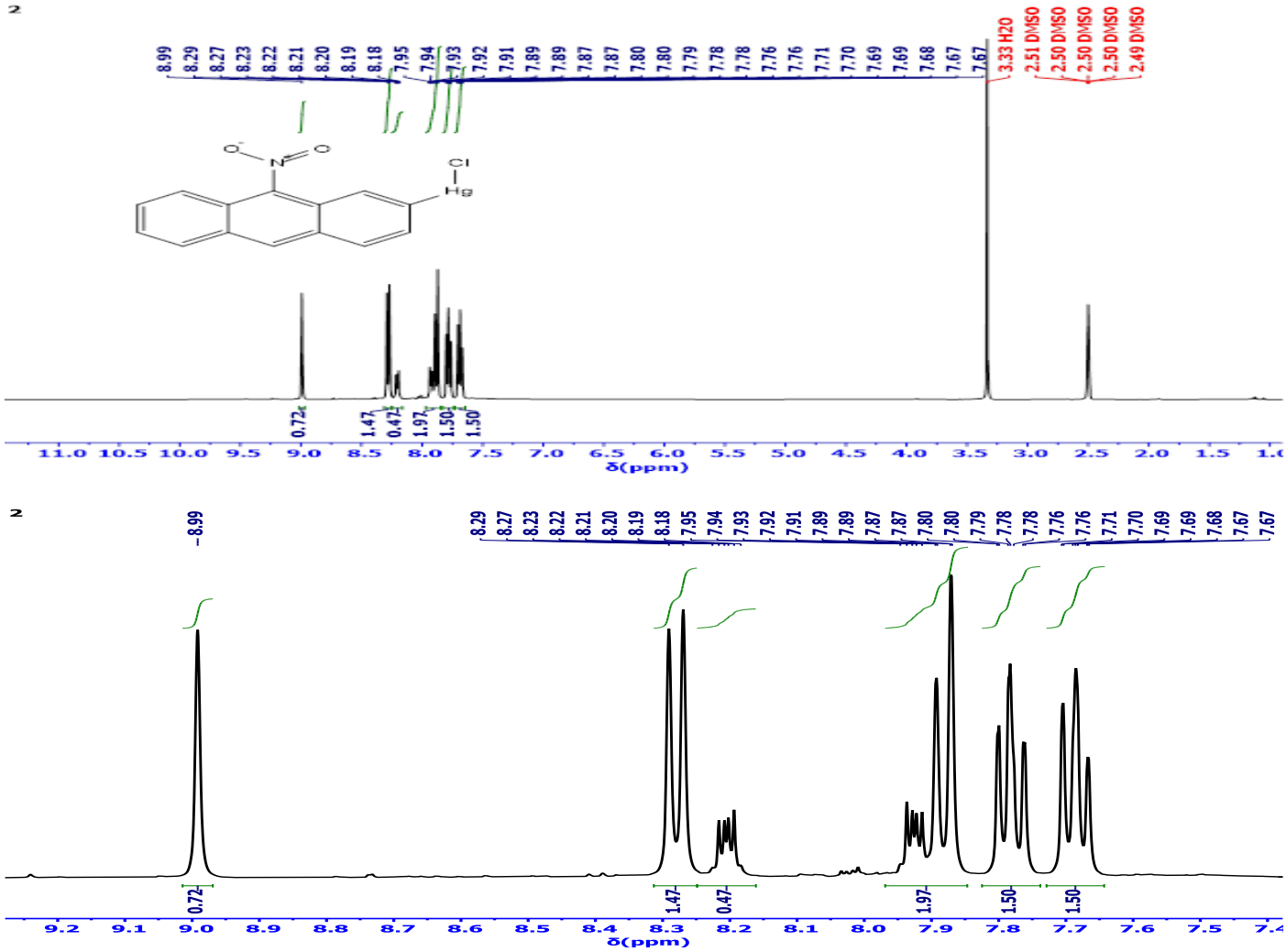

Fig S6. The ^{1}H NMR spectrum of compound B

x-ray diffraction

The Scherrer equation is related to the diffraction peak presented in Equation 10 where L is the size of the nanocrystal, K is the shape factor, which is typically taken as 0.89 for ceramic materials, λ is the wavelength of radiation in nanometers (K = 1.5406 nm), θ is the diffracted angle of the peak and β is the full width at half maximum of the peak in radians. Additionally, physical broadening and instrumental broadening are connected to peak broadening.

$$L = \frac{K\,\lambda}{\beta\,\cos\theta} \qquad (10)$$

For decreasing this error of instrument, Equation 11 can be used:

$$\beta_d^2 = \beta_m^2 - \beta_i^2 \qquad (11)$$

In this formula, β_m is the measured broadening, β_i is the instrumental broadening, and βd was introduced as the corrected broadening responsible for crystal size. With the aid of the adjustment for physical broadening, the full width half maximum (FWHM) measurement of the sample's instrumental and physical widening can be used to calculate the crystal size using the Scherrer equation.

The Scherrer equation only considers the impact of crystallite size on X-ray diffraction peak broadening; It does not take into account the inherent strain that develops in nanocrystals due to point defects, grain boundaries, triple junctions, and stacking faults. The Williamson Hall (W-H) approach, which also calculates the crystal size and the intrinsic strain, is one of the methods that takes the effect of strain-induced XRD peak broadening into account. The physical line broadening of the X-ray diffraction peak indicates that it is a result of both size and strain.

Table(S5) XRD data and average Crystal size of 1 calculated from average model in Scherrer equation

2θ (Degree)	θ (Degree)	$\cos\theta$ (Degree)	β = FWHM (Degree)	β = FWHM (Radian)	Crystal size $L = \frac{K\lambda}{\beta \cos\theta}$	Average crystal size (nm)
21.5296	10.7648	0.9824	0.462	0.008085	172.6281	126.9366
28.2782	14.1391	0.9697	0.3398	0.005947	237.7832	
32.3629	16.18145	0.9604	2.7814	0.048675	29.33096	
33.0543	16.52715	0.9587	0.3752	0.006566	217.8193	
40.3404	20.1702	0.9387	0.3768	0.006594	221.5155	
43.9951	21.99755	0.9272	0.5605	0.009809	150.7623	
46.4071	23.20355	0.9191	0.6962	0.012184	122.4461	
53.0071	26.50355	0.8949	1.4758	0.025827	59.32529	
58.3828	29.1914	0.873	0.5753	0.010068	156.0031	
63.1637	31.58185	0.8519	1.4749	0.025811	62.35778	
68.7725	34.38625	0.8252	2.2873	0.040028	41.51065	
76.048	38.024	0.7877	1.9218	0.033632	51.75744	

Table (S6) XRD data and average Crystal size of 2 calculated from average model in Scherrer equation

2θ (Degree)	θ (Degree)	$\cos\theta$ (Degree)	β = FWHM (Degree)	β = FWHM (Radian)	Crystal size $L = \frac{K\lambda}{\beta \cos\theta}$	Average crystal size (nm)
10.837	5.4185	0.9955	0.245	0.004288	321.2436	369.956
13.0544	6.5272	0.9935	0.286	0.005005	275.7452	
14.7141	7.35705	0.9917	0.2018	0.003532	391.5078	
19.7603	9.88015	0.9881	4	0.07	19.82353	
21.63	10.815	0.9822	0.3332	0.005831	239.407	
23.143	11.5715	0.9797	0.0362	0.000634	2209.226	
23.9867	11.99335	0.9782	0.2594	0.00454	308.7765	
27.1863	13.59315	0.972	0.2781	0.004867	289.8509	
28.3355	14.16775	0.9696	0.4636	0.008113	174.3034	
31.4346	15.7173	0.9626	0.3922	0.006864	207.5336	
32.9167	16.45835	0.959	1.5926	0.027871	51.2999	
35.0008	17.5004	0.9537	0.5466	0.009566	150.3005	
40.3103	20.15515	0.9387	1.0852	0.018991	76.91397	
43.9292	21.9646	0.9274	0.3462	0.006059	244.0325	
46.3751	23.18755	0.9192	0.5197	0.009095	164.0133	
51.2526	25.6263	0.9016	0.076	0.00133	1143.443	
52.4176	26.2088	0.8972	4	0.07	21.83195	

The W-H approach changes with tan in strain considerations rather than confirming a 1/cos dependency as in the Scherrer equation. This fundamental difference combines small crystallite size and microstrain in order to pursue a dissociation of broadening reflection. Equation provides the distinct correlations of the impacts of size and strain broadening in the analysis of W-H. (12).

$$\beta_{total} = \beta_{size} + \beta_{strain} \qquad (12)$$

Equation (13) was generated by the UDM approach to represent the strain connected to the nanocrystals:

$$\varepsilon = \frac{\beta}{4\ \tan\theta} = \frac{\beta_2\ \cos\theta}{4\ \sin\theta} \qquad (13)$$

Where β_2 is the broadening of the width of the peaks due to strain, while the broadening due to nanocrystal size β_1 comes from the Scherrer equation.

$$\beta = \beta_1 + \beta_2 = \frac{K\,\lambda}{L\,\cos\theta} + 4\,\varepsilon\,\frac{\sin\theta}{\cos\theta} \qquad (14)$$

$$\beta\,\cos\theta = \frac{K\,\lambda}{L} + 4\,\varepsilon\,\sin\theta \qquad (15)$$

From equation of straight line:

$$x = 4\sin\theta,\ y = \beta\,\cos\theta\,, slope = \varepsilon, intercept = \frac{K\,\lambda}{L}$$

When Plotting $4\sin\theta$ on the x-axis and $\beta\,\cos\theta$ on the y-axis (Table S8), we get the intercept representing $\frac{K\,\lambda}{L}$, from which we extract the crystal size.

$$L = \frac{K\,\lambda}{intercept} \qquad (16)$$

Table(S7) XRD data of 1 calculated from Williamson-Hall equation.

X= 4**sin** $\boldsymbol{\theta}$ (Degree)	Y= $\boldsymbol{\beta}$(Radian). **cos** $\boldsymbol{\theta}$(Degree)	Slope = strain, ε	Crystal size $\boldsymbol{L = \frac{K\,\lambda}{Intercept}}$
0.7472	0.007943	0.0088	415.5
0.9772	0.005767		
1.1148	0.046747		
1.138	0.006295		
1.3792	0.00619		
1.498	0.009095		
1.576	0.011198		
1.7848	0.023113		
1.9508	0.008789		
2.0948	0.021988		
2.2708	0.033031		
2.464	0.026492		

Table(S8) XRD data of 2 calculated from Williamson-Hall equation.

X= 4$\sin\theta$ (Degree)	Y= β(Radian). $\cos\theta$(Degree)	Slope = strain, ε	Crystal size $L = \frac{K\lambda}{Intercept}$
0.3776	0.004269	0.0092	285.65
0.4548	0.004972		
0.5124	0.003503		
0.6864	0.069167		
0.7504	0.005727		
0.8024	0.000621		
0.8312	0.004441		
0.94	0.004731		
0.9788	0.007866		
1.0836	0.006607		
1.1332	0.026728		
1.2028	0.009123		
1.378	0.017827		
1.496	0.005619		
1.5748	0.00836		
1.73	0.001199		
1.7664	0.062804		

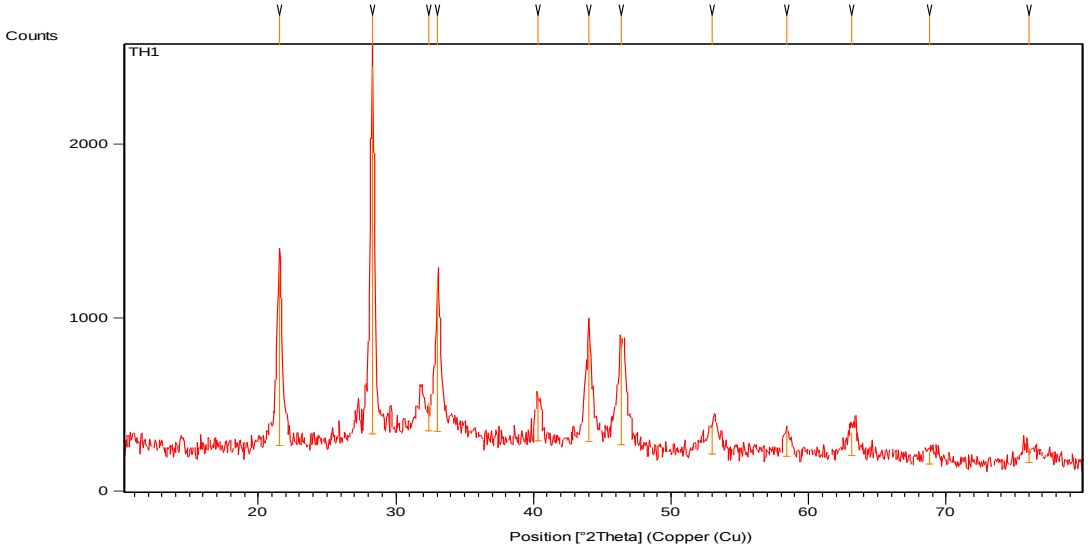

Fig S7 .The XRD of compound A

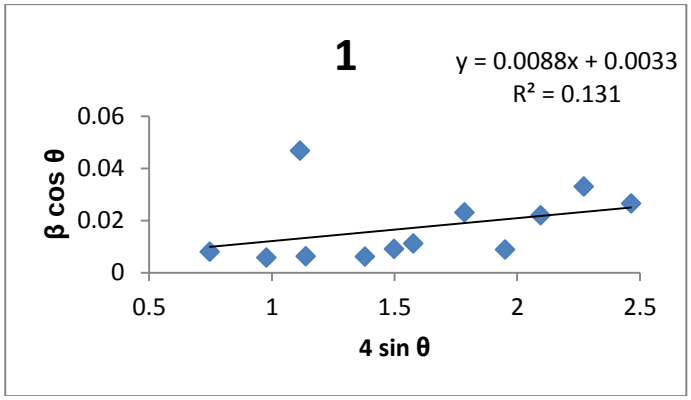

Fig S8. Williamson-Hall plot of the complex1.

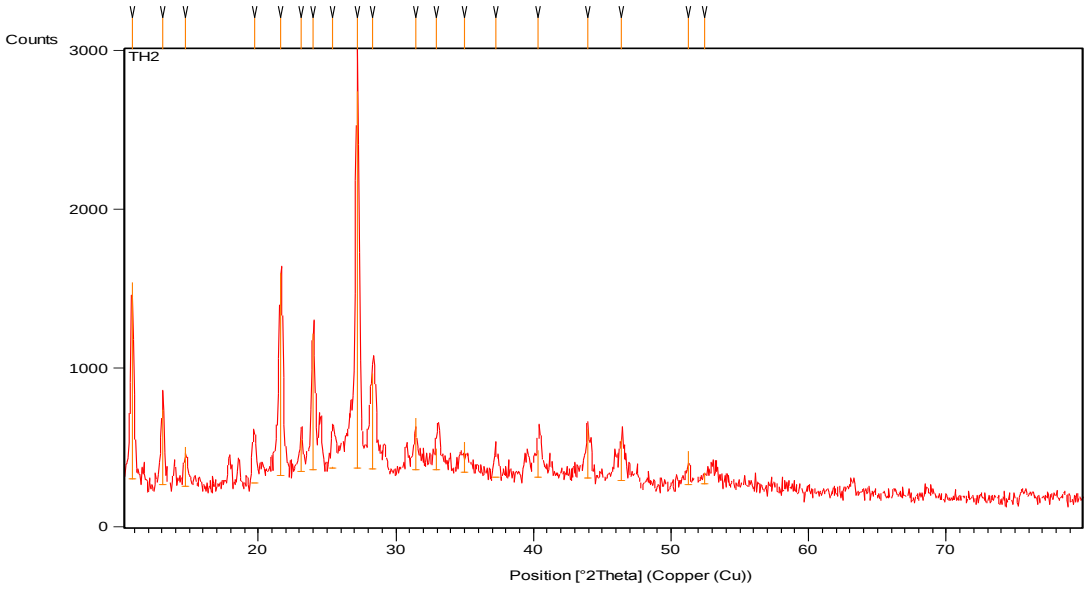

Fig S9. The XRD of compound A

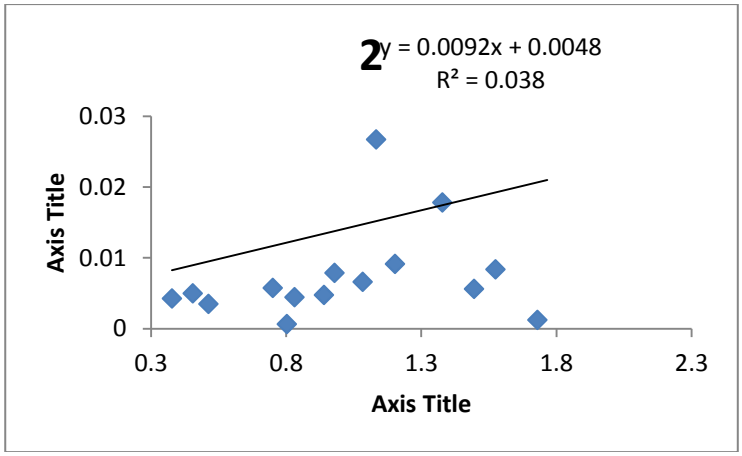

Fig S10 . Williamson-Hall plot of the complex 2

Antioxidants

Oxidative stress plays a major pivotal role in the etiology of many diseases of aging and many degenerative diseases, such as atherosclerosis, cardiovascular disease, type II diabetes and cancer [18]. In order to deal with the excess of free radicals producing oxidative stress, endogenous and exogenous mechanisms have been put in place in order to maintain redox

balance. Free radical scavenging is one of the best known mechanisms for evaluating antioxidant activity. The DPPH (short for Diphenyl-picrylhydrazyl organic compound) test A standardized test in an activity study Antioxidants It provides a rapid technique for screening the free radical scavenging process of specific compounds or extracts. A standard DPPH solution of purple color is prepared with a maximum absorbance at 517 nm. Antioxidant molecules deal with radicals in DPPH by providing hydrogen atoms or electrons through a free radical attack on the DPPH molecule and transforming it from purple to yellow as in Figure (S11).) leading to lower absorbance than 517 nm [19].

Figure (S11) DPPH changes color from purple to yellow

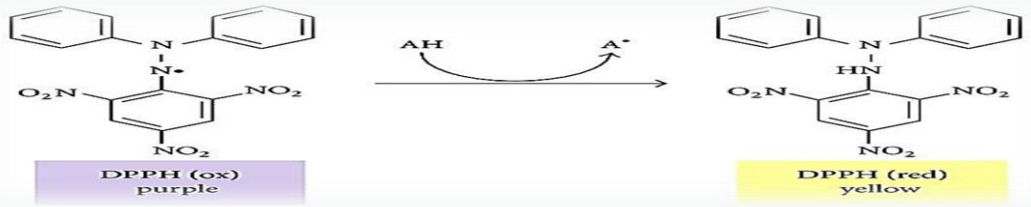

Figure (S12) shows the mechanism of hydrogen acquisition by the compound DPPH from other compounds [20,21].

Thus, the lower the rate of absorption more quickly, the greater the antioxidant activity in the compound, and the antioxidant activity was determined in the laboratory spectrophotometrically by DPPH radicals. On opposing oxidative challenges, the effectiveness of the compounds was calculated by applying the relationship (8-4) [22,23] , (8-4) .....% for DPPH to scavenge free radicals = (1-At) /A0 * 100 where:-

At = represents the absorbance of the remaining part of DPPH after adding the compound

Ao = is the absorbance of a standard DPPH solution .

Table (S8) values of the compounds towards DPPH and its comparison with standard ascorbic acid

DPPH inhibition	Concentration				Ascorbic acide
	0.001 M	0.002 M	0.003 M	0.004 M	
A	78.43	69.32	62.47	50.01	32.16
B	79.29	70.01	63.49	51.88	34.09

Conclusion

In the present study, compounds A and B were obtained in a 69 and 12.8% yield. All the prepared compounds were characterized by the mass spectrum, proton NMR, XRD and FTIR. Findings from this study were in concordance with previous research findings, confirming the correctness of the proposed structures for all the prepared compounds.

References

[1] J. D. Blum, L. S. Sherman, and M. W. Johnson, “Mercury isotopes in earth and environmental sciences,” *Annu. Rev. Earth Planet. Sci.*, vol. 42, pp. 249–269, 2014.

[2] M. Di-isobutyl, “Jan., 1929,” vol. 1880, no. 1879, pp. 1–4, 1929.

[3] B. F. Azevedo, L. B. Furieri, F. M. Pecanha, G.A. Wiggers, P.F. Vassallo, M.R. Simoes, J. Fiorim, P. R. de Batista, M. Fioresi, L. Rossoni, "Toxic effects of mercury on the cardiovascular and central nervous systems," *J. Biomed. Biotechnol.*, vol. 2012, 2012.

[4] J. F. Risher, H. E. Murray, and G. R. Prince, "Organic mercury compounds: Human exposure and its relevance to public health," *Toxicol. Ind. Health*, vol. 18, no. 3, pp. 109–160, 2002.

[5] P. Charvát, L. Klimeš, J. Pospíšil, J. J. Klemeš, and P. S. Varbanov, "An overview of mercury emissions in the energy industry - A step to mercury footprint assessment," *J. Clean. Prod.*, vol. 267, p. 122087, 2020.

[6] L. Aljerf, "Mercury Toxicity: Ecological Features of Organic Phase of Mercury in Biota- Part I," *Arch. Org. Inorg. Chem. Sci.*, vol. 3, no. 2, 2018.

[7] M. Sakamoto, M. Nakamura, and K. Murata, "Mercury as a Global Pollutant and Mercury Exposure Assessment and Health Effects," *Nihon Eiseigaku Zasshi.*, vol. 73, no. 3, pp. 258–264, 2018.

[8] R. C. Larock, "Mercury in Organic Chemistry. V. The Direct Esterification of Alkyl Halides," *J. Org. Chem.*, vol. 39, no. 25, pp. 3721–3727, 1974.

[9] Aziz, F.K., Gazar, S.H., and Al-Saadawy, N.H., 2020, Simple, selective, and sensitive spectrophotometric method for determination of trace amounts of lead(II), cadmium(II), cobalt(II) with organomercury compounds, *J. Global Pharma Technol.*, 12, 248–255.

[10] Silverstein, R. M., & Bassler, G. C., 1962, Spectrometric identification of organic compounds, *Journal of Chemical Education*, 39(11), 546.

[11] Ahmed, W.M., Al-Saadawy, N.H., and Abowd, M.I., 2021, Synthesis and characterization of a new organoselenium and organotellurium compounds depending on 9-

chloro-10-nitro-9,10-dihydroanthracene, *Ann. Romanian Soc. Cell Biol.*, 25 (4), 11035–11043..

[12] Pavia, D.L., Lampman, G.M., Kriz, G.S., and Vyvyan, J.A., 2014, *Introduction to Spectroscopy*, Cengage Learning, Boston, US.

[13] Al-Saadawy, N.H., 2022, New organotellurium compounds based on camphor, aniline and p-toluidine: Preparation, characterization and theoretical study, *Egypt. J. Chem.*, 65 (2), 19–27.

[14] McWhinnie, W.R., and Thavornyutikarn, P., 1972," A spectroscopic examination of phenyltellurium trihalides" *J. Chem.SOC. Dalton*,(4), 551- 554.

[15] Boursas, F., Berrah, F., Kanagathara, N., Anbalagan, G., and Bouacida, S., 2019, "XRD, FT-IR, FT-Raman spectrum and ab initio HF vibrational analysis of bis (5-amino-3-carboxy-1H-1, 2, 4-triazol-4-ium) selenate dihydrate," *J. Mol. Struct.*, 1180, 532–541.

[16] Scheinmann, F., 2013, An Introduction to Spectroscopic Methods for the Identification of Organic Compounds: Mass Spectrometry, Ultraviolet Spectroscopy,Electron Spin Resonance Spectroscopy, Nuclear Magnetic Resonance Spectroscopy (Recent Developments), Use of Various Spectral Methods Together, and Documentation of Molecular Spectra, Elsevier Science, Amsterdam, Netherlands.

[17] Al-Saadawy, N. H., 2022, "Synthesis, Characterization, and Theoretical Study of Some New Organotellurium Compounds Derived from Camphor," *Indones. J. Chem.*, 22(2), 442.

[18] K. K. Griendling, L. L. Camargo, F. J. Rios, R. Alves-Lopes, A. C. Montezano, and R. M. Touyz, "Oxidative Stress and Hypertension," *Circ. Res.*, pp. 993–1020, 2021.

[19] I. Aziz and N. Arifah, "Antioxidant Activity Using DPPH & Frap Method and Their Correlation with The Levels of Phenolic and Flavonoid Compounds from Nemba Plants (Azadirachta Indica A . Juss)," vol. 3, no. 2, pp. 10–20, 2020.

[20]B. B. de Menezes, L. M. Frescura, R. Duarte, M. A. Villetti, and M. B. da Rosa, "A critical examination of the DPPH method: Mistakes and inconsistencies in stoichiometry and IC50 determination by UV–Vis spectroscopy," *Anal. Chim. Acta*, vol. 1157, p. 338398, 2021.

[21] A. L. Dawidowicz, D. Wianowska, and M. Olszowy, "On practical problems in estimation of antioxidant activity of compounds by DPPH method (Problems in estimation of antioxidant activity)," *Food Chem.*, vol. 131, no. 3, pp. 1037–1043, 2012.

[22] F. Xiao, T. Xu, B. Lu, and R. Liu, "Guidelines for antioxidant assays for food components," *Food Front.*, vol. 1, no. 1, pp. 60–69, 2020 .

[23] L. Castaldo, L. Izzo, S. De Pascale, A. Narvaez, Y. Rodriguez-Carrasco, and A. Ritieni, "Chemical composition, in vitro bioaccessibility and antioxidant activity of polyphenolic compounds from nutraceutical fennel waste extract," *Molecules*, vol. 26, no. 7, 2021.